Antibody-secreting plasma cells persist for decades in human intestine

Ole J.B. Landsverk,[1] Omri Snir,[2] Raquel Bartolomé Casado,[1]* Lisa Richter,[1]* Jeff E. Mold,[5] Pedro Réu,[5,6] Rune Horneland,[7] Vemund Paulsen,[7] Sheraz Yaqub,[8] Einar Martin Aandahl,[4,7] Ole M. Øyen,[7] Hildur Sif Thorarensen,[9] Mehran Salehpour,[10] Göran Possnert,[10] Jonas Frisén,[5] Ludvig M. Sollid,[3]** Espen S. Baekkevold,[1]** and Frode L. Jahnsen[1]**

[1]Department of Pathology, Centre for Immune Regulation, [2]Department of Immunology, Centre for Immune Regulation, [3]Department of Immunology, Centre for Immune Regulation and KG Jebsen Coeliac Disease Research Centre, and [4]Centre for Molecular Medicine Norway, Nordic European Molecular Biology Laboratory Partnership, Oslo University Hospital-Rikshospitalet and The University of Oslo, 0372 Oslo, Norway
[5]Department of Cell and Molecular Biology, Karolinska Institute, 171 77 Stockholm, Sweden
[6]Center for Neuroscience and Cell Biology, University of Coimbra, 3000-213 Coimbra, Portugal
[7]Department of Transplantation Medicine and [8]Department of Gastrointestinal Surgery, Oslo University Hospital-Rikshospitalet, 0372 Oslo, Norway
[9]Department of Informatics, University of Oslo, 0313 Oslo, Norway
[10]Department of Physics and Astronomy, Ion Physics, Uppsala University, 752 36 Uppsala, Sweden

Plasma cells (PCs) produce antibodies that mediate immunity after infection or vaccination. In contrast to PCs in the bone marrow, PCs in the gut have been considered short lived. In this study, we studied PC dynamics in the human small intestine by cell-turnover analysis in organ transplants and by retrospective cell birth dating measuring carbon-14 in genomic DNA. We identified three distinct PC subsets: a CD19$^+$ PC subset was dynamically exchanged, whereas of two CD19$^-$ PC subsets, CD45$^+$ PCs exhibited little and CD45$^-$ PCs no replacement and had a median age of 11 and 22 yr, respectively. Accumulation of CD45$^-$ PCs during ageing and the presence of rotavirus-specific clones entirely within the CD19$^-$ PC subsets support selection and maintenance of protective PCs for life in human intestine.

INTRODUCTION

Plasma cells (PCs) in the gut produce antibodies that are transported into the gut lumen and provide crucial protection against enteric microbiota. PCs are derived from B cells that have been primed and undergone class-switch recombination in gut-associated lymphoid tissues (Pabst, 2012). The intestine is exposed to a changing repertoire of microbial and dietary antigens and must continuously adapt by adjusting its immune repertoire. In an early study in mice, the half-life of gut PCs was estimated to be 4.7 d (Mattioli and Tomasi, 1973), leading to the prevailing notion that the intestinal PC repertoire is highly dynamic and temporally restricted in antigen specificity. However, in mice, specific antibodies could be detected 112 d after transient exposure to *Escherichia coli* (Hapfelmeier et al., 2010), and PCs generated after immunization with cholera toxin were found to persist in the lamina propria for up to 9 mo (Lemke et al., 2016). In humans, the existence of long-lived PCs in the gut is inferred from their survival in vitro for 4 wk in cultured small intestinal biopsies (Mesin et al., 2011), their phenotypic and transcriptomal similarity with BM PCs (Nair et al., 2016), and the persistence of nonproliferating PCs in both ileum and colon for 234 d after CD19-directed chimeric antigen receptor T cell therapy (Bhoj et al., 2016). However, direct evidence of long-term persistence of human gut PCs is lacking.

RESULTS AND DISCUSSION

We used fluorescent in situ hybridization probes targeting X/Y chromosomes to discriminate between donor and recipient cells in biopsies from transplanted duodenum after mixed-gender pancreatic–duodenal transplantation (Ptx) of type I diabetes mellitus patients (Horneland et al., 2015) and found that most CD38$^+$ PCs remained of donor origin 1 yr after transplantation (Fig. 1 A). To investigate the characteristics of these persisting PCs, we applied a flow cytometry–based strategy on single-cell suspensions from duodenal-proximal jejunum (small intestine [SI]). SI resections were obtained during Whipple procedure (pancreatoduodenectomy) or from donor and recipient during Ptx. PCs were identified as CD38^{hi}CD27^{hi}CD138$^+$CD20$^-$ large cells, and we found that, in all adult subjects, they could be subdivided into three major subsets defined by selective expression of CD19 and CD45 (Fig. 1 B, top; Di Niro et al., 2010). For comparison,

*R.B. Casado and L. Richter contributed equally to this paper.

**L.M. Sollid, E.S. Baekkevold, and F.L. Jahnsen contributed equally to this paper.

Correspondence to Ole J.B. Landsverk: ole.jorgen.bjarnason.landsverk@rr-research.no; or Frode L. Jahnsen: frode.lars.jahnsen@rr-research.no

Abbreviations used: BCMA, B cell maturation antigen; PC, plasma cell; Ptx, pancreatic–duodenal transplantation; RM-ANOVA, repeated measures ANOVA; SI, small intestine; VLP, virus-like particle.

The Rockefeller University Press $30.00
J. Exp. Med. 2017 Vol. 214 No. 2 309–317
https://doi.org/10.1084/jem.20161590

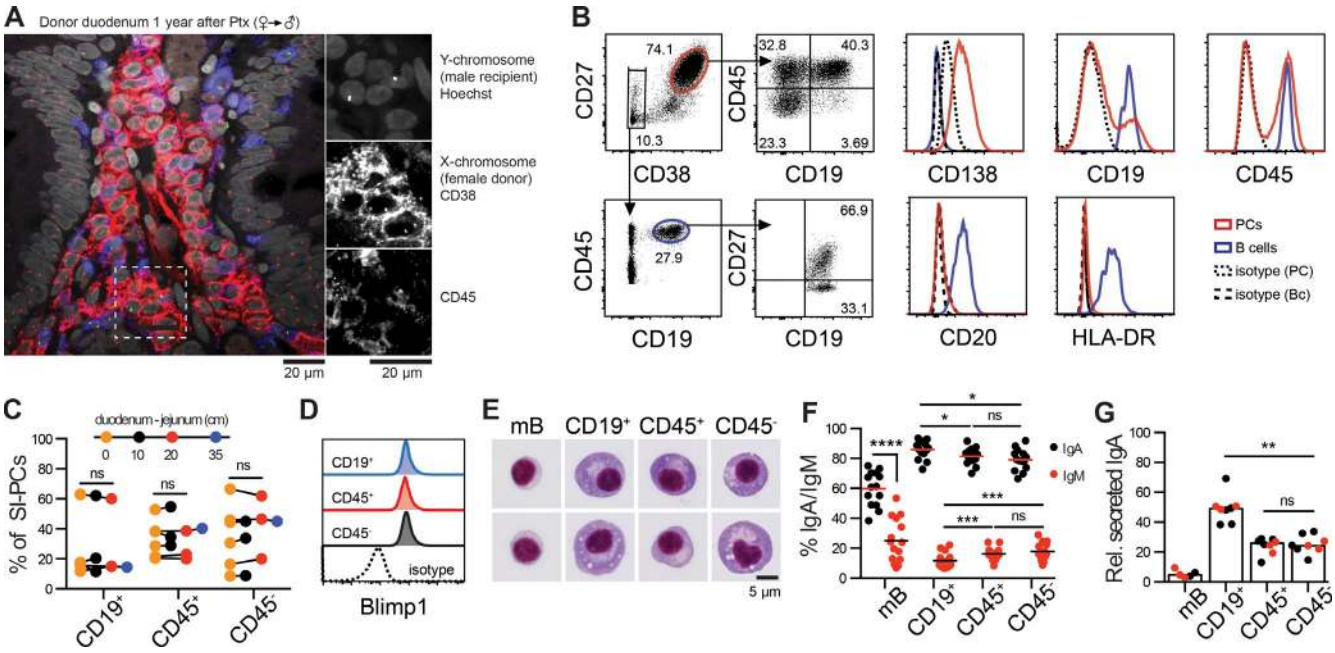

Figure 1. **PCs survive for 1 yr and comprise three distinct subsets in human SI.** (A) Immunofluorescence confocal micrograph of endoscopic biopsy from (female) donor duodenum 1 yr after Ptx into male recipient. Tissue sections were probed with X/Y chromosome fluorescent in situ hybridization probes (Y, green; X, red) and stained with anti-CD38 (red) and anti-CD45 (blue). Hoechst (gray) stains individual nuclei. The micrograph is representative of five gender-mismatched transplants. (B) Representative flow cytometric analysis of PCs (top) and B cells (bottom) from resected SI obtained during Whipple procedure or donor/recipient SI during Ptx. Dot plots and histograms are representative of all (CD27, CD38, CD19, and CD45), 4 (CD138), 19 (HLA-DR), and 5 (CD20) subjects. (C) The lengthwise representation of the PC subsets was determined by flow cytometric analysis of biopsies taken at intervals along resected duodenum-proximal jejunum from individual subjects after Whipple procedure. $n = 5$; paired Student's t test 0–20 cm ($n = 3$). (D) Blimp-1 expression among PC subsets was analyzed by intracellular staining and flow cytometry. The histogram is representative for 12 subjects (Whipple procedure). (E) Representative micrographs of memory B cells and PC subsets sorted by flow cytometry and stained with Hemacolor reagent. $n = 2$; Whipple procedure. (F) The percentage of memory B cells and PC subsets expressing cell surface IgA (black dots; $n = 14$) or IgM (red dots; $n = 15$) was determined by flow-cytometric analysis. Bars indicate median values. Dots represent individual subjects, SI resections from Whipple procedure, and Ptx. (G) IgA secretion from flow-sorted IgA^+ (black dots) or IgM^- (red dots) memory B and PC subsets was determined by ELISA after 40-h culture in vitro and was normalized to the total for each subject. $n = 5$; Whipple procedure and Ptx. (F and G) One-way repeated measures ANOVA (RM-ANOVA), IgA^+ versus IgM^+ memory B cells in F; paired Student's t test. *, $P \leq 0.05$; **, $P \leq 0.01$; ***, $P \leq 0.001$; ****, $P \leq 0.0001$. Bc, B cell; mB, memory B cell; Rel., relative.

we also examined $CD38^-CD20^+HLA\text{-}DR^+$ B cells. These were dominantly $CD27^+IgD^-$ memory B cells, consistently present at low frequency in SI lamina propria, whereas $CD27^-IgD^+IgM^+$ naive-mature B cells represented a variable minor contribution from isolated lymphoid follicles (Fig. 1 B, bottom; and not depicted; Farstad et al., 2000). The $CD19^+CD45^+$ (hereafter $CD19^+$) and two $CD19^-$ PC subsets (hereafter $CD45^+$ and $CD45^-$) had a similar representation in mucosal biopsies taken at intervals along the upper SI of individual subjects (Fig. 1 C), expressed high levels of CD27, CD38, and the PC transcription factor Blimp-1, and had characteristic PC morphology (Figs. 1, D and E). The majority of cells were IgA^+ in all subsets (Fig. 1 F). However, $CD19^+$ PCs had a larger proportion of IgA^+ cells, and these secreted more IgA than either of the $CD19^-$ PC subsets when cultured in vitro (Fig. 1 G). This could indicate that $CD19^+$ PCs represented a more active PC subset potentially recently generated in response to current antigenic challenge.

To quantitatively determine the in vivo dynamics of the PC subsets, we exploited differences in HLA class I haplotype between donors and recipients after Ptx (Fig. 2 A). We found very few new (recipient) PCs in donor duodenum 3–6 wk after transplantation, and these were dominantly $CD19^+$ (Fig. 2 B). After 1 yr, a median 32% of the $CD19^+$ PCs was from the recipient, whereas the input into the $CD45^+$ PC subset remained minor (median 2.3%), and the contribution to the $CD45^-$ PC subset was negligible (median 0.01%). By comparison, B cells were largely replaced within 3–6 wk. However, some patients retained a few donor memory B cells even after 1 yr (Fig. 2, A and B, left), suggesting that these cells may also contribute to maintaining the clonal repertoire in humans (Lindner et al., 2012). We could not detect any donor B cells or PCs in the adjacent recipient duodenum (Fig. 2 C), demonstrating that there was no lateral mobility or propagation of donor PCs or B cells from solitary cells or from putative residual lymphoid tissue in the graft. To establish whether the new (recipient) PCs were adding to or

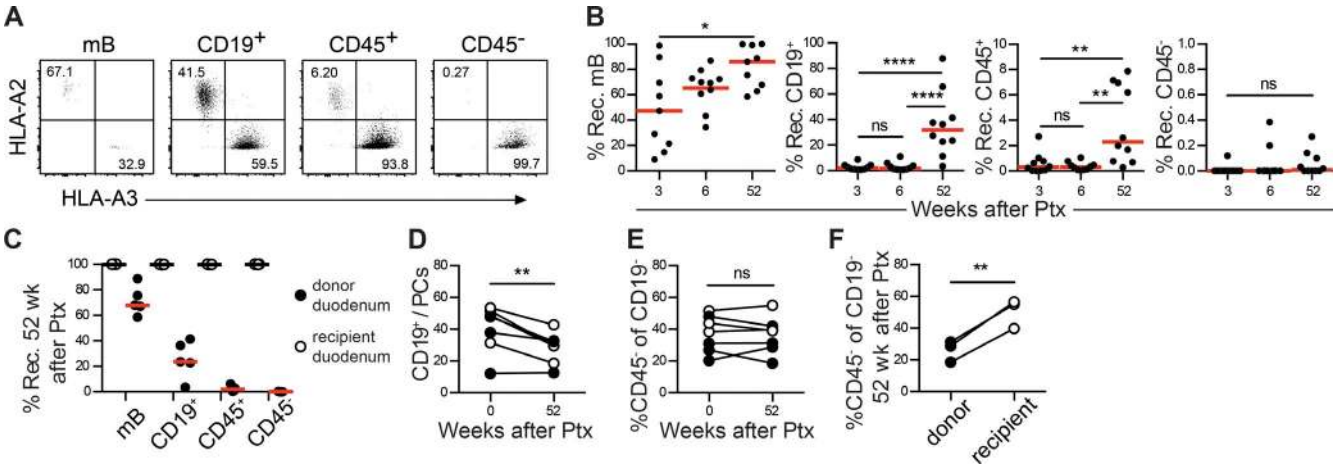

Figure 2. **SI-PC subsets have different replacement kinetics and in vivo stability.** (A) Representative flow cytometric analysis of memory B cell (mB) and PC subsets in endoscopic biopsies from donor duodenum 52 wk after Ptx (donor HLA-A2$^-$/A3$^+$; recipient HLA-A2$^+$/A3$^-$). (B) The percentage of recipient (Rec.) cells in each subset 3, 6, and 52 wk after Ptx was determined by HLA class I expression as in A. Each dot represents an individual donor. *n* = 10. One-way RM-ANOVA was used. (C) Chimerism was determined in endoscopic biopsies from donor duodenum (closed circles) and adjacent recipient duodenum (open circles) 52 wk after Ptx. *n* = 5. (D and E) The relative representation irrespective of origin of CD19$^+$ PCs among total PCs (D) and CD45$^-$ among CD19$^-$ PCs (E) was determined before and 52 wk after Ptx in donor (closed circles; *n* = 4) and adjacent recipient duodenum (open circles; *n* = 3). (F) Donor–recipients pairs with different CD19$^-$ PC subset representation before Ptx were examined 52 wk after transplantation (*n* = 3). Data points represent individual subjects; lines connect data from the same patients at different time points (D and E) or donor and recipient tissue at the same time point (F). Paired Student's *t* test was used. *, P ≤ 0.05; **, P ≤ 0.01; ****, P ≤ 0.0001.

replacing the preexisting donor CD19$^+$ PC population, we examined the relative representation of PC subsets (irrespective of origin) before and after Ptx. We observed a general decrease in CD19$^+$ PCs relative to the CD19$^-$ PC subsets after surgery in both donor and adjacent recipient duodenum (Fig. 2 D). However, the ratio between the CD19$^-$ PC subsets remained stable throughout the 1-yr follow-up (Fig. 2 E), and any difference in CD19$^-$ PC subset representation between donor and recipient before transplantation was maintained (Fig. 2 F). This demonstrates that CD19$^+$ PCs are dynamically exchanged in human SI and that the CD19$^-$ PC subsets represent stable populations with potentially very long lifespans that do not rapidly adapt to the environment of a new host.

The subdivision and dynamics of SI PCs are reminiscent of the recently reported division of BM PCs into static CD19$^-$ PCs that maintain long-term immunity and dynamic CD19$^+$ PCs that provide the transient response to new antigens (Halliley et al., 2015; Mei et al., 2015). In the BM, CD19$^-$ PCs have a prosurvival phenotype characterized by low expression of the proapoptotic receptor CD95, high expression of the antiapoptotic protein Bcl2, and low proliferation relative to CD19$^+$ PCs (Mei et al., 2015). We found that PCs in human SI had a similar phenotype: CD19$^+$ PCs expressed significantly more CD95, less Bcl-2, and contained more proliferating Ki67$^+$ cells relative to CD45$^-$ PCs, whereas CD45$^+$ PCs were intermediate in all regards (Fig. 3, A–C). BM PCs are maintained in a survival niche where a proliferation-inducing ligand (APRIL) binding to the B cell maturation antigen (BCMA) is a crucial survival factor (O'Connor et al., 2004; Peperzak et al., 2013). APRIL is abundantly present in human intestine (Barone et al., 2009; Gustafson et al., 2014), and we found that BCMA was highly expressed by all SI PC subsets (Fig. 3 D). Furthermore, homotypic interactions between CD56$^+$ osteoblasts and/or mesenchymal stem cells and PCs may be involved in stable positioning within the BM survival niche, and CD80/86 interaction with CD28 can support the survival of long-lived BM PCs (see Mei et al., 2015). CD56 and CD28 are both enriched in CD19$^-$ relative to CD19$^+$ PCs in the BM (Mei et al., 2015), and we found a similar distinction in the SI, with CD45$^+$ PCs expressing intermediate levels of both markers (Fig. 3, E and F). To determine whether pathogen-specific clones were contained among the long-lived SI PCs, we measured reactivity against eGFP-labeled rotavirus particles (Di Niro et al., 2010). Rotavirus infects a high proportion of the population worldwide and is a major cause of diarrhea in young children. It has previously been demonstrated that the SI contain PCs specific for rotavirus (Di Niro et al., 2010), and we found that rotavirus-specific clones were predominantly present within the CD19$^-$ PC subsets in all subjects tested (Fig. 3 G).

The intermediate phenotype and dynamics suggested that CD45$^+$ PCs represented a developmental stage between CD19$^+$ PCs and CD45$^-$ PCs. To elucidate the relationship between the SI-PC subsets, we sorted IgA$^+$ PCs from SI resections obtained from Whipple procedure and performed high throughput sequencing of the heavy-chain variable region (IGHV) genes. All PC subsets displayed similar IGVH gene segment usage and number of IGHV somatic mutations

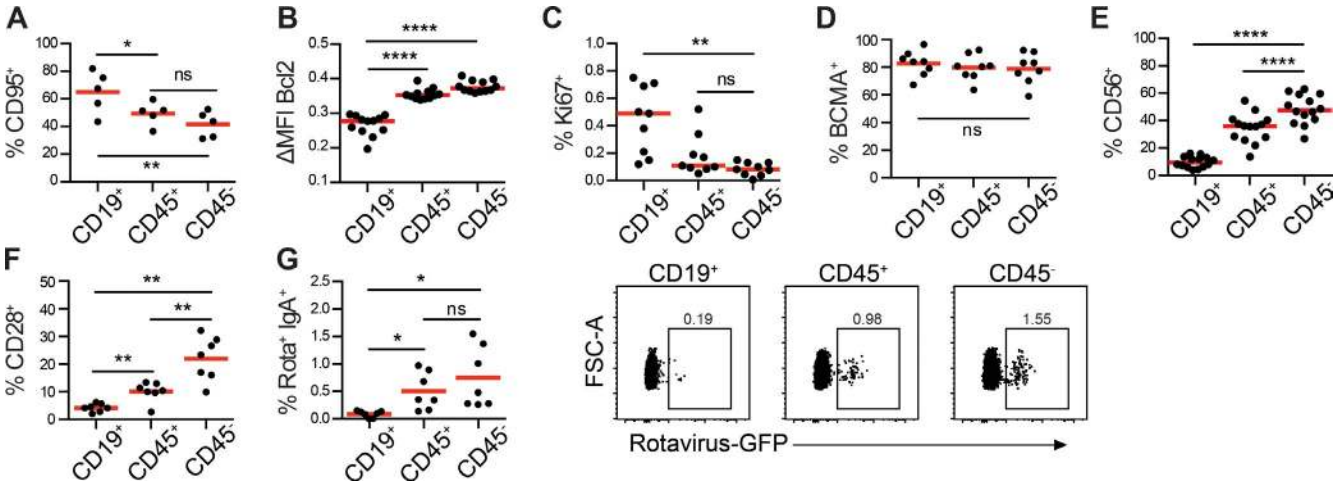

Figure 3. **CD19⁻ PCs exhibit features of advanced maturity and are enriched for rotavirus-specific clones.** (A) The percentage of CD95⁺ cells was determined relative to isotype control by flow cytometric analysis. $n = 5$; Whipple procedure. (B) The mean fluorescence intensity (MFI) of Bcl2 relative to isotype control staining (ΔMFI) on PC subsets was determined by flow cytometric analysis and presented as the fraction of total value for each subject. $n = 12$; Whipple procedure. (C–F) The percentage of Ki67⁺ ($n = 9$), BCMA⁺ ($n = 10$), CD56⁺ ($n = 14$), and CD28⁺ ($n = 7$) was determined relative to isotype control staining in SI resections (Whipple procedure and Ptx). (G) Rotavirus-reactive PCs were detected using eGFP-labeled VLPs relative to eGFP by flow cytometric analysis (SI resections from Whipple procedure [$n = 3$] or Ptx [$n = 4$]; median age 49 yr; range 7–74 yr; 2 female). Data points represent individual subjects. Red bars indicate mean values. FSC, forward side scatter. *, $P \leq 0.05$; **, $P \leq 0.01$; ****, $P \leq 0.0001$; one-way RM-ANOVA.

(Fig. 4, A and B). Application of the Morisita-Horn index showed an overall high degree of clonal sharing between the SI-PC subsets (Fig. 4 C). However, CD45⁻ PCs were consistently more closely related to CD45⁺ PCs than CD19⁺ PCs, and CD45⁺ PCs exhibited a higher level of clonal sharing with the other two subsets (Fig. 4, C and D), thus supporting an intermediate developmental stage of CD45⁺ PCs.

To investigate the development of the long-lived SI-PC compartment, we examined the representation of PC subsets in relation to age in SI resections obtained from donors ($n = 27$; age 7–51 yr; 17 female) and patients ($n = 18$; age 23–57 yr; 7 female) during Ptx and from patients undergoing Whipple procedure ($n = 27$; age 57–87 yr; 13 female). We found that whereas the CD19⁺ PCs were consistently present in all subjects, the CD19⁻ PC compartment was completely dominated by CD45⁺ PCs until late adolescence (Fig. 5, A and B). To directly determine the age of PCs in the SI, we sorted the PC subsets from resected SI (Whipple procedure) and measured carbon-14 in genomic DNA by accelerator mass spectrometry. The concentration of carbon-14 in DNA mirrors the level of atmospheric carbon-14, which peaked during the cold war and then decreased exponentially after the Limited Nuclear Test Ban Treaty in 1963 and can be used to retrospectively birth date cells in humans (Bergmann et al., 2009). We determined that the median age of CD45⁻ PCs was 22 yr among our subjects. CD45⁺ PCs were 11 yr old, whereas CD19⁺ PCs appeared to undergo constant renewal (Fig. 5 C). It is known that intestinal PCs are absent at birth but increase during the first few months to reach adult densities in early childhood (El Kaissouni et al., 1998; Gustafson et al., 2014). Therefore, subjects born before the bomb spike may have PCs formed early in life that contain low concentrations of carbon-14, and thus, the determined ages for these subjects represent lower limits of the actual age of the cells (Fig. 5 D). Furthermore, as the individual carbon-14 values were derived from several million sorted cells and cells were added to the PC compartment over time (Fig. 2 B and Fig. 5 A), the oldest cells in the population would likely be considerably older than the quantified average. In agreement with our other results, this suggests that there is a gradual selection and conservation of clones from the CD19⁺ PC population into a CD19⁻ PC compartment initially as CD45⁺ PCs that, after some time, lose CD45 expression. It is highly probable that clones generated during childhood, such as during rotavirus infection (Fig. 3 G), are maintained within the CD45⁻ PC population. To our knowledge, the expression of CD45 by CD19$^{+/-}$ BM PCs has not been addressed, but it is known that BM contains CD45$^{+/-}$ PCs, and as both CD19⁻ and CD45⁻ BM PCs express more CD56 and proliferate less than their positive counterparts, it seems likely that a similar division of PCs exists in the BM (Pellat-Deceunynck and Bataille, 2004; Mei et al., 2015).

In conclusion, we have defined three subsets of SI PCs, which are functionally and phenotypically similar to BM PCs, and delineated their distinct replacement kinetics and developmental relationship. The presence and persistence of long-lived SI PCs deviates from the prevailing paradigm of humoral memory in the gut. Our data indicate that current antigenic challenge and attrition primarily affects the dynamic CD19⁺ PC compartment and show that distinct antibody specificities are conserved within a very long-lived CD19⁻ PC population that likely provides life-long protection against enteric pathogens. The existence of long-lived,

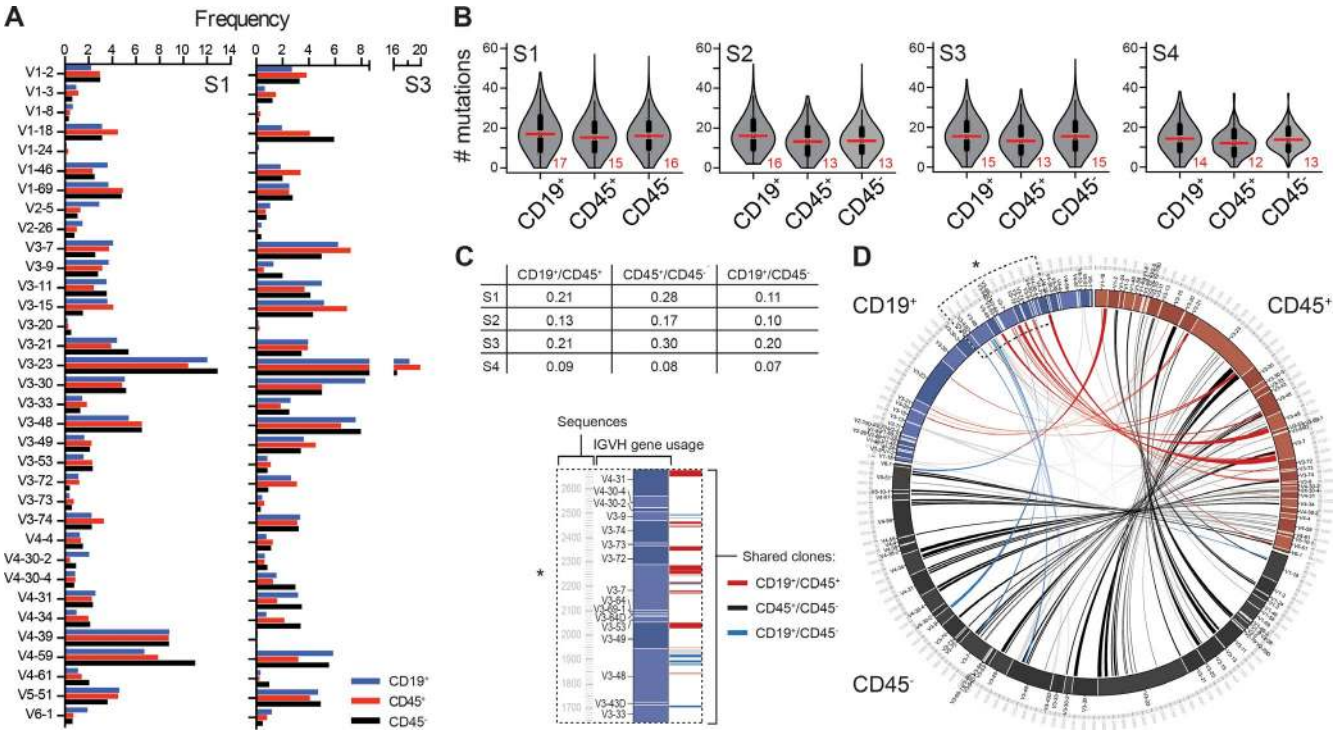

Figure 4. **Clonal relationships indicate selection and sequential development of SI PCs.** (A–D) High throughput sequencing was performed on FACS IgA$^+$ PC subsets from SI resections (n = 4; 2 female; mean age 70 yr, range 61–77 yr; Whipple procedure) and analyzed as described in the High throughput sequencing of IGHV section of Materials and methods. (A) The frequency of IGHV gene segments used by the PC subsets is shown for two representative subjects (S1 and S3). (B) The level of somatic hypermutation among PC subsets for sequenced subjects (S1–S4) is presented in violin plots. The median number of mutations is indicated on plots in red bars and numbers. (C) The data table gives Morisita-Horn indices for clonal similarity between PC subsets in sequenced subjects (S1–S4). (D) Clonally related sequences assigned between PC subsets illustrated in a Circos plot. Lines represent clones shared between CD19$^+$ and CD45$^+$ (red), CD45$^+$ and CD45$^-$ (black), CD19$^+$, and CD45$^-$ (blue) or all PC subsets (gray) above a threshold of ≥10 unique sequences for one representative subject (S3). The width of the lines is proportional to the number of unique sequences within single clones. The asterisk marks the zoomed in region (left) describing figure elements in the Circos plot.

nonproliferating CD19$^-$ PCs in the gut gives promise for the development of oral vaccines but also needs to be addressed in clinical strategies targeting malignant or autoreactive PCs using chemotherapy, therapeutic antibodies, and chimeric antigen receptor T cell therapy.

MATERIALS AND METHODS

Human biological material

Duodenum-proximal jejunum tissue was resected from non-pathological SI during Whipple procedure (pancreaticoduodenectomy) of pancreatic cancer, distal bile duct cancer, or periampullary carcinoma patients (n = 35; mean age 70 yr; range 53–87 yr; 17 female) or from donor and patient duodenum during pancreas transplantation of type I diabetes mellitus patients (donors: n = 21, mean age 25 yr, range 7–51 yr, 11 female; patients: n = 15, mean age 40 yr, range 23–57 yr, 6 female; Horneland et al., 2015). Endoscopic biopsies were obtained from donor and patient duodenum by endoscopy 3, 6, and 52 wk after transplantation. All biological samples were evaluated blindly by an experienced pathologist (F.L. Jahnsen), and only material with normal histology was included (Ruiz et al., 2010). Resected SI was opened longitudinally and rinsed thoroughly in PBS, and mucosal folds were dissected off the submucosa. Mucosal specimens for microscopy were fixed directly in formalin and paraffin embedded. To obtain single-cell suspensions for flow cytometry, cell sorting, and culture, epithelial cells were removed by washing in PBS containing 2 mM EDTA three times for 20 min at 37°C, and the lamina propria was minced and digested in RPMI medium containing 2.5 mg/ml Liberase and 20 U/ml DNase I (both from Roche) at 37°C for 1 h. Digested tissue was passed through 100-µm cell strainers (Falcon) and washed three times in PBS. The study was approved by the Regional Committee for Medical Research Ethics in Southeast Norway and the Privacy Ombudsman for Research at Oslo University Hospital–Rikshospitalet and complies with the Declaration of Helsinki. All participants gave their written informed consent.

Flow cytometry and FACS

Single-cell suspensions from lamina propria were analyzed by flow cytometry according to standard procedure using fluoro-

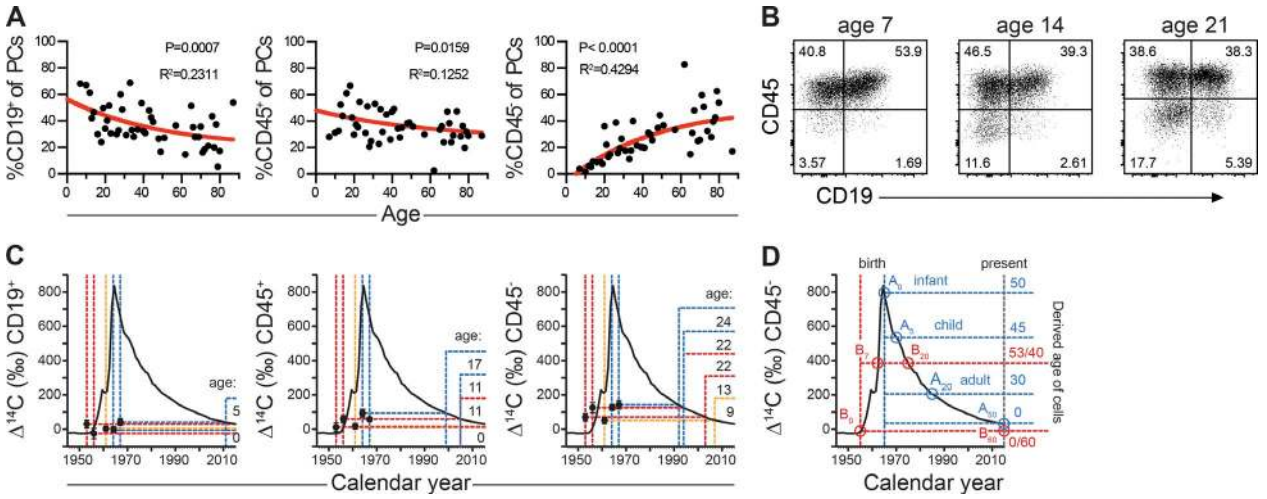

Figure 5. **CD45⁻ PCs accumulate with age and persist for decades in human SI.** (A) The representation of each SI-PC subset in SI resections (n = 72) obtained during Whipple procedure or donors and recipients during Ptx was determined by flow cytometric analysis and plotted against subject age. Lines represent nonlinear fitting (one-phase exponential decay). R^2 and two-tailed p-values of age and subset representation are shown on the graphs (Pearson correlation). (B) Dot plots show representative flow cytometric analysis of subjects with increasing age from A. (C) Carbon-14 concentrations in genomic DNA isolated from SI-PC subsets bead sorted from SI resections (Whipple procedure) were measured by accelerator mass spectrometry (n = 5; 1 female). The average age of cells in each PC subset was inferred from plotting the concentration of carbon-14 from each sample on the atmospheric carbon-14 curve, determining the corresponding year, and subtracting the year samples were acquired. Dots represent carbon-14 values and year of birth for individual donors. Vertical dashed red lines indicate data from subjects born before, yellow lines during the increase, and blue lines after the peak in atmospheric carbon-14. (D) Illustration of the strategy to infer age of cells based on amount of carbon-14 in genomic DNA relative to carbon-14 level in the atmosphere and subject age (hypothetical subject A [blue]; subscript gives age). Note that in subjects born prior to the bomb peak (red; B_0), cells generated during the bomb spike (i.e., B_7) will have higher carbon-14 concentration relative to their renewal rate, and cells generated post-bomb (i.e., B_{20} and B_{60}) will have lower carbon-14 concentration relative to their renewal rate.

chrome-conjugated antibodies targeting HLA-A2–PE (Abcam); CD20-FITC, CD45-APC-H7, and Ki67-FITC (BD); Bcl2–Alexa Fluor 488, BCMA-PE, CD3-APC, CD14-APC, CD19–Alexa Flour 488/PE-Cy7, CD20-PE, CD27-BV421/Pacific blue/APC-Cy7/PE-Cy7, CD28–Alexa Fluor 488, CD38-PE/APC-Cy7, CD45-BV510/APC-Cy7, CD56–Alexa Flour 488, CD95-PE, and HLA-DR–BV605/PerCP (BioLegend); CD138-FITC/PE-Cy7 and HLA-A3–FITC/APC (eBioscience); HLA-B7–PE (EMD Millipore); HLA-B8–PE (Miltenyi Biotec); IgA-FITC/PE, IgM-FITC/PE, and IgD-FITC/PE (Southern-Biotech); and Blimp-1–DyLight 488 (Thermo Fisher Scientific). For detection of intracellular antigens, cells were fixed in formaldehyde and permeabilized using a Foxp3 staining buffer set (eBioscience). Detection of rotavirus-specific PCs was performed using eGFP-tagged virus-like particle 2 (VLP2)–eGFP/VLP6 (provided by D. Poncet and A. Charpilienne, Institut de Biologie Integrative de la Cellule, Paris, France; Charpilienne et al., 2001) at a final concentration of 1 µg/ml. eGFP (Promega) was used as a negative control. All flow cytometry was performed on an LSRFortessa, and FACS was performed on a FACSAriaII flow cytometer (both from BD). Data were analyzed using FlowJo 10 (Tree Star), and figures were assembled in Illustrator CS4 (Adobe).

Microscopy

Sections were cut from paraffin blocks in series at 4 µm, mounted on Superfrost Plus object glasses (Thermo Fisher Scientific), and washed sequentially in xylene, ethanol, and PBS. Heat-induced epitope retrieval was performed by boiling sections for 20 min in Dako buffer and cooled to room temperature before staining. Sections were incubated with CEP X SpectrumOrange/Y SpectrumGreen DNA Probes (Abbott Molecular Inc.) for 12 h at 37°C before immunostaining according to standard protocol with anti-CD38 (clone SPC32; Novocastra), anti-CD45 (polyclonal; Abcam), and secondary antibodies targeting mouse IgG1 or rabbit IgG conjugated to Alexa Fluor 555 and 647, respectively. Stained sections were mounted with ProLong Diamond Antifade mountant (Molecular Probes). Sorted cells were attached to Superfrost Plus object glasses by centrifugation at 800 rpm for 3 min, stained with Hemacolor reagents (EMD Millipore), and mounted with Pertex mounting medium (Histolab Products AB). Light microscopy was conducted on a BX51 microscope (Olympus) using 10×/0.30 or 40×/0.75 UPlanFI objectives, and images were acquired with a Colorview IIIu camera (Olympus). Phase contrast micrographs of sorted cells cultured in vitro (Fig. S1 B, insets) were acquired on a microscope (DM IL; Leica Biosystems), with a 40×/0.50 Hi PLAN1 objective and a DCF290 camera (Leica Biosystems) using Cell^P software. Laser scanning confocal microscopy was performed on an Olympus FV1000 (BX61WI) system with 405-, 488-, 543-, and 633-nm laser lines using 20×/0.80 or 60×/1.35 UPlanSApo oil objectives (Olympus). Image z

stacks were acquired at 1-µm intervals and combined using the Z project max intensity function in Image J (National Institutes of Health). All microscopy images were assembled in Photoshop and Illustrator CS4 (Adobe).

Cell culture and ELISA

Cells were flow sorted as IgA^+ ($n = 5$) or IgM^- ($n = 3$) and cultured for 40 h in RPMI medium with 10% heat-inactivated fetal calf serum, L-glutamine, and penicillin-streptomycin at a density of 2.5×10^5 cells/ml before cells were spun down at 500 rcf/7 min, and the supernatant was transferred in twofold dilution to 96-well plates precoated with rabbit anti–human IgA (A0262; Dako) and blocked with 1% BSA. Purified IgA monomer at known concentration was used as standard (courtesy of R. Iversen, Oslo University Hospital-Rikshospitalet and the University of Oslo, Oslo, Norway). Bound IgA was detected with goat anti–human IgA peroxidase conjugate (A0295; Sigma-Aldrich) and tetramethylbenzidine (Kirkegaard & Perry Laboratories).

High throughput sequencing of IGHV

10^4 IgA^+ cells of each subset from four donors were sorted into 25 µl of catch buffer (10 mM dithiothreitol and 2 U/µl RNAsin [Promega] in PBS) and snap frozen at −80°C. cDNA synthesis was performed using IGHJ reverse primers indexed to allow simultaneous sequencing of different samples, as well as six random nucleotides to generate unique molecular identifiers and a part of Illumina adapters (Snir et al., 2015). 3.5 µl of 10 µM indexed IGHJ primer was added together with 1.5% vol/vol NP-40 and 0.5 µl of 40 U/µl RNAsin (Promega) to 14 µl of lysate. Diethylpyrocarbonate-treated water was added to a final volume of 25 µl, and lysates together with primer mix were incubated at 65°C for 5 min. Next, 25 µl of reverse transcriptase mix (10 µl × 5 reverse transcriptase buffer, 3.5 µl of 100 mM dithiothreitol, 4.5 µl of 10 mM dNTP-Mix, 0.7 µl of 40 U/µl RNAsin [Promega], 0.9 µl Superscript III [Invitrogen], and diethylpyrocarbonate-treated water) was added. cDNA was synthesized at 42°C for 10 min, 25°C for 10 min, 50°C for 60 min, and 94°C for 5 min and stored at −20°C. Second-strand cDNA was synthesized using AmpliTaq Gold polymerase (Applied Biosystems) with forward IGHV1–6 framework region 2 (van Dongen et al., 2003), which was indexed and included six random nucleotides and a part of Illumina adapters. Second-strand synthesis was performed at 95°C for 7.5 min, 52°C for 2 min, and 72°C for 10 min. Double-stranded cDNA was further purified using an AMPure XP system (Beckman Coulter) at a 1:1 ratio according to the manufacturer's instructions. Next, the second part of the Illumina adapter was connected using R1 and R2 primers. PCR was performed using Multiplex PCR (QIA GEN) at 95°C for 15 min × 25 (95°C for 30 s, 60°C for 45 s, and 72°C for 90 s) and 72°C for 10 min. Final IGHV amplicon libraries were purified using the AMPure XP system and further run and extracted from agarose gel. Paired-end sequencing of 300 base pairs was performed using a MiSeq sequencer (Illumina) at the Norwegian Sequencing Centre in Oslo, Norway. Raw sequencing data were processed using pRESTO (Vander Heiden et al., 2014) as previously described (Snir et al., 2015). Unique sequences to which at least two copies were present were further aligned using the ImMunoGeneTics database (Lefranc et al., 2003), and their IGHV, IVHJ segments, and CDR3 were determined (Table S1). Clonally related sequences originating from a common ancestor were assigned within the PC subsets and between the different subsets using Change-O (Gupta et al., 2015), and the frequencies of clones that are shared between PCs subsets was further calculated. Presentation of clonal sharing between PC subsets was assembled in Circos (Krzywinski et al., 2009), where the size of each subset is determined based on the number of clones and duplicates within each subset. A threshold of 10 duplicates was applied for lines to be drawn between individual shared clones, and the width of connecting lines is proportional to the number of duplicates within single clones.

Bead-based PC sorting for carbon-14 dating

Single-cell suspensions from SI resections ($n = 6$; Whipple procedure; Table S2) were stained with biotinylated (DSB-X Biotin Protein kit; Molecular Probes) anti-CD38 antibody (clone HB7 from Absolut Antibody LTd). Bead-free $CD38^+$ cells were obtained after isolation with Flexicomp beads and subsequent incubation with releasing buffer, following the kit's instructions (11061D; Thermo Fisher Scientific). Rare contaminating $CD38^{dim}$ T cells were depleted with anti-CD3 Dynabeads (11151D; Thermo Fisher Scientific) before release of $CD38^+$ PCs. Purity of sorted $CD38^+$ PCs was assessed by flow cytometry and was consistently >90%. $CD19^+$, $CD45^+$, and $CD45^-$ PC subsets were magnetic-activated cell sorted in two sequential steps: first applying CD19 microbeads and, then, sorting the resulting negative fraction with CD45 microbeads (both from Miltenyi Biotec).

DNA extraction for carbon-14 dating

A clean room (ISO8) was used to isolate the DNA. All glassware was baked for 4 h at 450°C before use. The cells were incubated at 65°C overnight with 1 ml of lysis buffer (100 mM Tris, pH 8.0, 200 mM NaCl, 1% SDS, and 5 mM EDTA) and 12 µl of 40 mg/ml proteinase K. 6 µl of RNase cocktail (Ambion) was added and incubated at 65°C for 1 h. Half a volume of 5 M NaCl was added to each sample. The tubes were vortexed for 30 s and then spun down at 13,000 rpm for 6 min. The supernatant was transferred to a glass vial containing absolute ethanol (three times the volume) and then gently agitated. The DNA was washed three times in washing buffer (70% ethanol [vol/vol] and 0.5 M NaCl) and dried at 65°C overnight. 500 µl of DNase/RNase free water (Gibco; Invitrogen) was used to resuspend the DNA. The purity and concentration were verified by UV spectroscopy (NanoDrop; Table S2).

Accelerator mass spectrometry and carbon-14 dating

A special sample preparation method has been developed for the microgram-sized DNA samples (Salehpour et al., 2013).

The purified DNA samples were received suspended in water. The samples were subsequently lyophilized to dryness under vacuum and centrifugation. Excess CuO was added to the dried samples in quartz tubes, which were then evacuated and sealed with a high temperature torch. The quartz tubes were placed in a furnace set at 900°C for 3.5 h to combust all carbon to CO_2. The evolved gas was cryogenically purified and trapped. The CO_2 gas was converted to graphite in individual submilliliter reactors at 550°C for 6 h in the presence of zinc powder as reducing agent and iron powder as catalyst. The graphite targets were measured at the Department of Physics and Astronomy, Ion Physics, Uppsala University using a 5-MV pelletron tandem accelerator (Salehpour et al., 2015). Stringent and thorough laboratory practice is necessary to minimize the introduction of stray carbon into the samples, including preheating of all glassware and chemicals before sample preparation. Large CO_2 samples (>100 µg) were split and $\delta^{13}C$ was measured by stable isotope ratio mass spectrometry, which established the $\delta^{13}C$ correction to $-24.1 \pm 1\%$ (2 SD) for leukocyte samples. Corrections and reduction of background contamination introduced during sample preparation were made as described by Hua et al. (2004) and Santos et al. (2007). The measurement error was determined for each sample and ranged between ± 8 and 24% (2 SD) $\Delta^{14}C$ for the large sample and small samples (10 µg C), respectively. All ^{14}C data are reported as decay corrected $\Delta^{14}C$ or Fraction Modern. All accelerator mass spectrometry analyses were performed blind to age and origin of the sample. Carbon-14 data are summarized in Table S2.

Statistical analysis

All statistical analysis was performed in Prism 6 (GraphPad Software). Statistical significance between subsets was calculated using Tukey's posthoc test for multiple comparisons. Paired Student's *t* test with two-tailed p-value (95% confidence interval) was used to compare ratios of PCs. Nonlinear fitting was applied using one-phase association. Correlation between age and subset abundance was calculated using Pearson correlation with two-tailed p-value (95% confidence interval). Morisita-Horn index for similarity between different subsets was calculated using the R spa package. Results are expressed as individual data points with median or mean values ± SD. P-values of <0.05 were considered significant. The tests used and magnitudes for p-values are indicated in each figure legend.

Online supplemental material

Fig. S1 presents gating strategy for flow cytometry and cell sorting. Table S1 provides additional IGHV sequencing data, and Table S2 presents detailed carbon-14 data.

ACKNOWLEDGMENTS

We thank J. Spencer for critical review of the manuscript. We are grateful to A. Aursjø, K. Thorvaldsen, and K. Hagelsteen for technical assistance, S. Nygård for help with violin plots, R. Iversen for providing purified sIgA, Didier Poncet and Annie Charpilienne for providing the rotavirus-like particles, K. Håkansson and P. Senneryd for AMS sample preparation, Katrin Lundin and Christian Naper (Oslo University Hospital-Rikshopitalet, Oslo, Norway) for providing HLA-typing, and the Confocal Microscopy and Flow Cytometry Core Facilities at Oslo University Hospital–Rikshopitalet.

This study was supported by grants from the Research Council of Norway through its Centres of Excellence funding scheme (project number 179573), South-Eastern Norway Regional Health Authority, the Swedish Research Council, the Swedish Cancer Society, the Karolinska Institute, Tobias Stiftelsen, the Strategic Research Program in Stem Cells and Regenerative Medicine at Karolinska Institute, Knut och Alice Wallenbergs Stiftelse, and Torsten Söderbergs Stiftelse. P. Réu was supported by a grant from the Foundation for Science and Technology from the Portuguese government (SFRH/BD/33465/2008). J.E. Mold was supported by a Human Frontiers Science Program Long-Term Fellowship (LT-000231/2011-L).

The authors declare no competing financial interests.

Author contributions: O.J.B. Landsverk, E.S. Baekkevold, and F.L. Jahnsen conceived the project. O.J.B. Landsverk designed and performed all experiments and analysis of all data except where otherwise specified, processed most biopsies, designed all figures, and wrote the manuscript. O. Snir performed RNA extraction, IGHV synthesis and isolation, and IGHV sequence analysis, performed flow cytometry analysis with rotavirus-like particles, and provided critical insights. R.B. Casado developed and performed bead-based isolation of PC subsets for carbon-14 measurements and processed biopsies. L. Richter processed biopsies, assisted with statistical analysis, and provided critical insights. J.E. Mold, P. Réu, M. Salehpour, G. Possnert, and J. Frisén contributed to study design and data analysis relating to carbon-14 measurements. J. Frisén supervised carbon-14 studies. R. Horneland, O.M. Øyen, and E.M. Aandahl recruited patients that were subjected to pancreas transplantation, coordinated endoscopic biopsies and blood samples, performed transplantation, and provided tissue material. S. Yaqub recruited patients with pancreatic cancer, performed surgery, and organized material from Whipple procedure. R. Horneland, O.M. Øyen, and E.M. Aandahl performed transplantations and provided material. V. Paulsen performed endoscopic examination and provided endoscopic biopsies. H.S. Thorarensen developed programming to generate Circos plots. F.L. Jahnsen, L.M. Sollid, and E.S. Baekkevold supervised the study. O. Snir, L. Richter, R.B. Casado, J.E. Mold, P. Réu, J. Frisén, L.M. Sollid, E.S. Baekkevold, and F.L. Jahnsen contributed to writing the manuscript.

Submitted: 22 September 2016
Revised: 28 November 2016
Accepted: 13 December 2016

REFERENCES

Barone, F., P. Patel, J.D. Sanderson, and J. Spencer. 2009. Gut-associated lymphoid tissue contains the molecular machinery to support T-cell-dependent and T-cell-independent class switch recombination. *Mucosal Immunol.* 2:495–503. http://dx.doi.org/10.1038/mi.2009.106

Bergmann, O., R.D. Bhardwaj, S. Bernard, S. Zdunek, F. Barnabé-Heider, S. Walsh, J. Zupicich, K. Alkass, B.A. Buchholz, H. Druid, et al. 2009. Evidence for cardiomyocyte renewal in humans. *Science.* 324:98–102. http://dx.doi.org/10.1126/science.1164680

Bhoj, V.G., D. Arhontoulis, G. Wertheim, J. Capobianchi, C.A. Callahan, C.T. Ellebrecht, A.E. Obstfeld, S.F. Lacey, J.J. Melenhorst, F. Nazimuddin, et al. 2016. Persistence of long-lived plasma cells and humoral immunity in individuals responding to CD19-directed CAR T-cell therapy. *Blood.* 128:360–370. http://dx.doi.org/10.1182/blood-2016-01-694356

Charpilienne, A., M. Nejmeddine, M. Berois, N. Parez, E. Neumann, E. Hewat, G. Trugnan, and J. Cohen. 2001. Individual rotavirus-like particles containing 120 molecules of fluorescent protein are visible in living cells. *J. Biol. Chem.* 276:29361–29367. http://dx.doi.org/10.1074/jbc.M101935200

Di Niro, R., L. Mesin, M. Raki, N.Y. Zheng, F. Lund-Johansen, K.E. Lundin, A. Charpilienne, D. Poncet, P.C. Wilson, and L.M. Sollid. 2010. Rapid generation of rotavirus-specific human monoclonal antibodies from small-intestinal mucosa. *J. Immunol.* 185:5377–5383. http://dx.doi.org/10.4049/jimmunol.1001587

El Kaissouni, J., M.C. Bene, S. Thionnois, P. Monin, M. Vidailhet, and G.C. Faure. 1998. Maturation of B cells in the lamina propria of human gut and bronchi in the first months of human life. *Dev. Immunol.* 5:153–159. http://dx.doi.org/10.1155/1998/42138

Farstad, I.N., H. Carlsen, H.C. Morton, and P. Brandtzaeg. 2000. Immunoglobulin A cell distribution in the human small intestine: phenotypic and functional characteristics. *Immunology.* 101:354–363. http://dx.doi.org/10.1046/j.1365-2567.2000.00118.x

Gupta, N.T., J.A. Vander Heiden, M. Uduman, D. Gadala-Maria, G. Yaari, and S.H. Kleinstein. 2015. Change-O: a toolkit for analyzing large-scale B cell immunoglobulin repertoire sequencing data. *Bioinformatics.* 31:3356–3358. http://dx.doi.org/10.1093/bioinformatics/btv359

Gustafson, C.E., D. Higbee, A.R. Yeckes, C.C. Wilson, E.F. De Zoeten, P. Jedlicka, and E.N. Janoff. 2014. Limited expression of APRIL and its receptors prior to intestinal IgA plasma cell development during human infancy. *Mucosal Immunol.* 7:467–477. http://dx.doi.org/10.1038/mi.2013.64

Halliley, J.L., C.M. Tipton, J. Liesveld, A.F. Rosenberg, J. Darce, I.V. Gregoretti, L. Popova, D. Kaminiski, C.F. Fucile, I. Albizua, et al. 2015. Long-lived plasma cells are contained within the $CD19^{-}CD38^{hi}CD138^{+}$ subset in human bone marrow. *Immunity.* 43:132–145. http://dx.doi.org/10.1016/j.immuni.2015.06.016

Hapfelmeier, S., M.A. Lawson, E. Slack, J.K. Kirundi, M. Stoel, M. Heikenwalder, J. Cahenzli, Y. Velykoredko, M.L. Balmer, K. Endt, et al. 2010. Reversible microbial colonization of germ-free mice reveals the dynamics of IgA immune responses. *Science.* 328:1705–1709. http://dx.doi.org/10.1126/science.1188454

Horneland, R., V. Paulsen, J.P. Lindahl, K. Grzyb, T.J. Eide, K. Lundin, L. Aabakken, T. Jenssen, E.M. Aandahl, A. Foss, and O. Øyen. 2015. Pancreas transplantation with enteroanastomosis to native duodenum poses technical challenges—but offers improved endoscopic access for scheduled biopsies and therapeutic interventions. *Am. J. Transplant.* 15:242–250. http://dx.doi.org/10.1111/ajt.12953

Hua, Q., U. Zoppi, A. Williams, and A. Smith. 2004. Small-mass AMS radiocarbon analysis at ANTARES. *Nucl. Instrum. Methods Phys. Res. B.* 223–224:284–292. http://dx.doi.org/10.1016/j.nimb.2004.04.057

Krzywinski, M., J. Schein, I. Birol, J. Connors, R. Gascoyne, D. Horsman, S.J. Jones, and M.A. Marra. 2009. Circos: an information aesthetic for comparative genomics. *Genome Res.* 19:1639–1645. http://dx.doi.org/10.1101/gr.092759.109

Lefranc, M.P., C. Pommié, M. Ruiz, V. Giudicelli, E. Foulquier, L. Truong, V. Thouvenin-Contet, and G. Lefranc. 2003. IMGT unique numbering for immunoglobulin and T cell receptor variable domains and Ig superfamily V-like domains. *Dev. Comp. Immunol.* 27:55–77. http://dx.doi.org/10.1016/S0145-305X(02)00039-3

Lemke, A., M. Kraft, K. Roth, R. Riedel, D. Lammerding, and A.E. Hauser. 2016. Long-lived plasma cells are generated in mucosal immune responses and contribute to the bone marrow plasma cell pool in mice. *Mucosal Immunol.* 9:83–97. http://dx.doi.org/10.1038/mi.2015.38

Lindner, C., B. Wahl, L. Föhse, S. Suerbaum, A.J. Macpherson, I. Prinz, and O. Pabst. 2012. Age, microbiota, and T cells shape diverse individual IgA repertoires in the intestine. *J. Exp. Med.* 209:365–377. http://dx.doi.org/10.1084/jem.20111980

Mattioli, C.A., and T.B. Tomasi. 1973. The life span of IgA plasma cells from the mouse intestine. *J. Exp. Med.* 138:452–460. http://dx.doi.org/10.1084/jem.138.2.452

Mei, H.E., I. Wirries, D. Frölich, M. Brisslert, C. Giesecke, J.R. Grün, T. Alexander, S. Schmidt, K. Luda, A.A. Kühl, et al. 2015. A unique population of IgG-expressing plasma cells lacking CD19 is enriched in human bone marrow. *Blood.* 125:1739–1748. http://dx.doi.org/10.1182/blood-2014-02-555169

Mesin, L., R. Di Niro, K.M. Thompson, K.E. Lundin, and L.M. Sollid. 2011. Long-lived plasma cells from human small intestine biopsies secrete immunoglobulins for many weeks in vitro. *J. Immunol.* 187:2867–2874. http://dx.doi.org/10.4049/jimmunol.1003181

Nair, N., E.W. Newell, C. Vollmers, S.R. Quake, J.M. Morton, M.M. Davis, X.S. He, and H.B. Greenberg. 2016. High-dimensional immune profiling of total and rotavirus VP6-specific intestinal and circulating B cells by mass cytometry. *Mucosal Immunol.* 9:68–82. http://dx.doi.org/10.1038/mi.2015.36

O'Connor, B.P., V.S. Raman, L.D. Erickson, W.J. Cook, L.K. Weaver, C. Ahonen, L.L. Lin, G.T. Mantchev, R.J. Bram, and R.J. Noelle. 2004. BCMA is essential for the survival of long-lived bone marrow plasma cells. *J. Exp. Med.* 199:91–98. http://dx.doi.org/10.1084/jem.20031330

Pabst, O. 2012. New concepts in the generation and functions of IgA. *Nat. Rev. Immunol.* 12:821–832. http://dx.doi.org/10.1038/nri3322

Pellat-Deceunynck, C., and R. Bataille. 2004. Normal and malignant human plasma cells: proliferation, differentiation, and expansions in relation to CD45 expression. *Blood Cells Mol. Dis.* 32:293–301. http://dx.doi.org/10.1016/j.bcmd.2003.12.001

Peperzak, V., I. Vikström, J. Walker, S.P. Glaser, M. LePage, C.M. Coquery, L.D. Erickson, K. Fairfax, F. Mackay, A. Strasser, et al. 2013. Mcl-1 is essential for the survival of plasma cells. *Nat. Immunol.* 14:290–297. http://dx.doi.org/10.1038/ni.2527

Ruiz, P., H. Takahashi, V. Delacruz, E. Island, G. Selvaggi, S. Nishida, J. Moon, L. Smith, T. Asaoka, D. Levi, et al. 2010. International grading scheme for acute cellular rejection in small-bowel transplantation: single-center experience. *Transplant. Proc.* 42:47–53. http://dx.doi.org/10.1016/j.transproceed.2009.12.026

Salehpour, M., K. Håkansson, and G. Possnert. 2013. Accelerator mass spectrometry of ultra-small samples with applications in the biosciences. *Nucl. Instrum. Methods Phys. Res. B.* 294:97–103. http://dx.doi.org/10.1016/j.nimb.2012.08.054

Salehpour, M., K. Håkansson, and G. Possnert. 2015. Small sample accelerator mass spectrometry for biomedical applications. *Nucl. Instrum. Methods Phys. Res. B.* 361:43–47. http://dx.doi.org/10.1016/j.nimb.2015.04.047

Santos, G.M., J.R. Southon, S. Griffin, S. Beaupre, and E. Druffel. 2007. Ultra small-mass AMS 14C sample preparation and analyses at KCCAMS/UCI Facility. *Nucl. Instrum. Methods Phys. Res. B.* 259:293–302. http://dx.doi.org/10.1016/j.nimb.2007.01.172

Snir, O., L. Mesin, M. Gidoni, K.E. Lundin, G. Yaari, and L.M. Sollid. 2015. Analysis of celiac disease autoreactive gut plasma cells and their corresponding memory compartment in peripheral blood using high-throughput sequencing. *J. Immunol.* 194:5703–5712. http://dx.doi.org/10.4049/jimmunol.1402611

Vander Heiden, J.A., G. Yaari, M. Uduman, J.N. Stern, K.C. O'Connor, D.A. Hafler, F. Vigneault, and S.H. Kleinstein. 2014. pRESTO: a toolkit for processing high-throughput sequencing raw reads of lymphocyte receptor repertoires. *Bioinformatics.* 30:1930–1932. http://dx.doi.org/10.1093/bioinformatics/btu138

van Dongen, J.J., A.W. Langerak, M. Brüggemann, P.A. Evans, M. Hummel, F.L. Lavender, E. Delabesse, F. Davi, E. Schuuring, R. García-Sanz, et al. 2003. Design and standardization of PCR primers and protocols for detection of clonal immunoglobulin and T-cell receptor gene recombinations in suspect lymphoproliferations: report of the BIOMED-2 Concerted Action BMH4-CT98-3936. *Leukemia.* 17:2257–2317. http://dx.doi.org/10.1038/sj.leu.2403202